THE ASTROPHYSICAL JOURNAL, 261:183–194, 1982 October 1

THE TWO-PHOTON CONTINUUM IN HERBIG-HARO OBJECTS

M. A. DOPITA AND L. BINETTE
Mount Stromlo and Siding Spring Observatories, Research School of Physical Sciences, Australian National University
AND
R. D. SCHWARTZ[1]
Department of Physics, University of Missouri, St. Louis
Received 1981 October 21; accepted 1982 April 9

ABSTRACT

The blue continuum seen in many Herbig-Haro (HH) objects is shown to be intrinsic to the source, and is due to a collisionally excited two-photon continuum of hydrogen. We find a strong inverse correlation between its strength and the excitation class of the HH spectrum. The most likely explanation of the data, based on theoretical models is that both the lines and continuum arise in a shock of finite age running into a partially preionized medium, so that if HH shocks are excited by a stellar wind from a pre–main-sequence star, this wind is likely to be episodic rather than continuous.

Subject headings: nebulae: general — shock waves — stars: pre–main-sequence — stars: winds

I. INTRODUCTION

The discovery of "excess" blue-violet continua in Herbig-Haro (HH) objects 1 and 2 (Böhm, Schwartz, and Siegmund 1974) has since been confirmed (Brugel, Böhm, and Mannery 1981*a*), and the continua have been found to increase into the satellite UV from *IUE* investigations (Ortolani and D'Odorico 1980; Böhm, Böhm-Vitense, and Brugel 1981). The character of these continua appears to be fundamentally different from that contained in HH 24, for example, where the continuum is predominantly red and possesses high polarization (Strom, Strom, and Kinman 1974; Schmidt and Miller 1979). Whereas HH 24 is an example of an object with combined reflection and emission components (Schwartz 1975; Schmidt and Miller 1979), most HH objects (including HH 1 and 2) exhibit little if any visual continuum or polarization, suggesting that they are intrinsic emission nebulae. Thus the presence of the blue-UV continuum in excess of what is expected either from recombination processes in nebular emission or from the reflection of the continuum of a nearby T Tauri star has been a source of mystery.

In this paper we report the results of spectrophotometric studies of nine HH objects covering a wide range of excitation class. Details of the observations are presented in §§ II–IV and the character of the well-defined continuous spectra is interpreted in § V. A discussion of the results and remaining problems occurs in § VI.

II. OBSERVATIONS

The optical spectra were obtained under photometric conditions at the Anglo-Australian 3.9 m Telescope on the nights of 1981 January 7–8 and 8–9. The Royal Greenwich Observatory Spectrograph was used with its 25 cm camera and the Image Photon Counting System (IPCS) (Boksenburg 1972) as detector. A grating of 250 lines mm^{-1} blazed in the blue was used in first order with a slit width of 400 μm (2″.65 on the sky), giving a spectral resolution of 11 Å (just sufficient to resolve the [S II] doublet) and a spectral coverage of 3000–7500 Å. The external memory was used to give 50 spectra each 2044 pixels long separated by 2″.07 on the sky.

These spectra were reduced by the following procedure. First, pixel to pixel variations were removed by the division of the data by a normalized flat field obtained by a long exposure of a tungsten lamp, unfiltered, in the third order red. Second, each spectrum was rebinned and made linear in wavelength by making a two-dimensional third order polynomial fit to the calibration arcs. Third, the mean of those spectra adjudged to be free of nebular or stellar contributions was subtracted from each spectrum to correct for the sky. Fourth, the spectra were converted to absolute flux by correcting for extinction and multiplication by a smooth response function, corrected for 2nd order blue leak in the region $\lambda > 6300$ Å, obtained from observations of Oke (1974) white dwarf standard stars with and without a RG 580 filter. The blue leak is less than 5% with this grating, but, in view of the possible contamination of the continuum data, we have not attempted to measure continuum intensities beyond 6300 Å. Finally, means of the spectra of individual knots were obtained by adding all the spectra in which the knot was detected.

The spectrophotometry resulting from this procedure is considered to be of very high quality and shows a good degree of internal consistency from one exposure to the next. A systematic error may arise in the case of the very strongest lines due to saturation of the

[1] Visiting Fellow, Australian National University.

TABLE 1

OBSERVED (F) AND REDDENING CORRECTED (F_0) FLUXES IN HH OBJECTS

		HH 1NW		HH 1SE		HH 2A		HH 2B		HH 2G	
Ident.	λ (Å)	F	F_0	F	F_0	F	F_0	F	F_0	F	F_0
[OII]	3727,9	133.7	225.2	141	237	117.1	175.5	287.8	431.4	165	245
H10	3797,9	3.4	5.5	2.7	4.4	3.8	5.6	3.5	5.1	3.0	4.4
H9	3835,4	5.4	8.6	4.5	7.2	6.0	8.6	5.8	8.3	5.4	7.8
H8, HeI, [NeIII]	3868	12.0	18.8	9.0	14.1	22.9	32.5	12.5	17.7	11.1	15.8
Hε, HeI	3889	11.3	17.6	8.4	13.0	15.1	21.3	10.5	14.8	9.4	13.2
CaII	3934	18.2	27.7	24.0	36.5	12.2	16.9	22.0	30.5	20.5	28.4
CaII [NeIII]	3968	29.7	44.4	25.1	37.4	29.7	40.6	26.8	36.6	28.5	38.9
[SII]	4068,76	87.0	124	81.6	116.4	76.6	101	52.5	68.9	63.3	83.4
Hδ	4100	18.9	26.6	16.1	22.5	22.1	28.8	19.3	25.1	19.6	25.5
[FeII]	4245	9.8	13.1	8.8	11.6	8.9	11.0	5.6	6.9	9.6	11.9
[FeII]	4276,87	10.8	14.0	7.1	9.2	9.9	12.1	10.7	13.1	11.4	13.9
Hγ	4340	35.5	44.7	41.0	51.6	44.4	53.3	39.1	46.7	37.8	45.2
[OIII],[FeII]	4363	11.6	14.5	8.6	10.7	12.4	14.7	6.3	7.5	13.0	15.4
[FeII]	4415	10.2	12.5	9.2	11.2	9.8	11.4	10.8	12.6	11.1	12.9
[MgI], FeII	4562,71	8.7	9.9	10.6	12.1	5.8	6.4	7.4	8.2	8.8	9.7
HeII	4686	-	-	-	-	8.2	8.7	9.3	9.9	6.1	6.5
Hβ	4861	100		100		100		100		100	
[OIII]	4959	18.4	17.7		12.5	36.0	35.0	18.8	18.3	15.9	15.4
[OIII]	5007	57.3	54.55	43	40.7	94.0	90.0	56.7	54.2	43.0	41.2
[FeII]	5158	28.0	24.9	28.8	25.6	21.7	19.8	18.3	16.9	28.5	26.0
[NI]	5198,200	22.5	19.6	60.2	52.5	12.4	11.1	20.6	18.5	27.8	25.0
[FeII]	5261,73	18.3	15.5	9.9	8.4	18.5	16.3	14.0	12.3	21.6	19.0
[FeII]	5334	5.6	4.6	5.8	4.8	7.1	6.1	1.9	1.6	5.0	4.3
[FeII]	5528	8.2	6.3	8.0	6.2	8.7	7.1	2.7	2.2	8.6	7.0
[NII]	5755	8.9	6.3	7.3	5.2	12.7	9.7	6.4	4.9	7.8	6.0
HeI	5876	11.2	7.7	7.3	5.0	15.2	11.3	6.6	4.9	6.4	4.8
[OI]	6300	230	141	472	289	215	147	180	123	236	162
[OI]	6363	100	59	165	97.6	86.8	57.7	70.1	46.6	87.0	58.9
[NII]	6548	62	34.9	112	63.1	82.5	52.8	78.9	50.5	64.0	41.0
Hα	6563	540	302	600	335.6	516	328.7	512.7	326.6	484.6	308.7
[NII]	6583	254	141	365	203	257	163	267.7	169.8	226.8	143.9
HeI	6678	2.7	1.5	2.6	1.4	3.9	2.4	2.8	1.7	-	-
[SII]	6717	126	67.7	328	176	121.6	75.1	245.3	151.4	129	79.6
[SII]	6731	236	126.4	488	261	183.5	113	284.6	175.2	231	142.2
HeI	7065	-	-	-	-	7.5	4.4	-	-	-	-
[FeII]	7155	-	-	-	-	53.3	30.5	28.8	16.5	54	30.9
[FeII]	7172	68	32.8	61	29.4	12.1	6.9	4.4	2.5	11	6.2
[CaII]	7291	103	48.8	120	56.8	54.1	30.3	65.8	36.8	79	44.2
[OII],[FeII]	7318,30	176	82.8	141	66.3	233.2	130	128.5	71.5	130	72.4
FeII, NiII	7376	42	19.6	35	16.3	39.6	21.9	22.7	12.6	30	16.6
C_{SO}		0.565		0.847		0.642		0.630		0.495	
C_{Bal}		0.667		0.947		0.444		0.589		0.660	
C_{adopt}		0.76		0.76		0.59		0.59		0.59	

IPCS. Lines likely to be affected are Hα and [O II] in HH 2H and [O II] in HH 1 NW. In general, relative line intensities of lines of similar strength to Hβ should be accurate to about 10%, except in the region longward of 7000 Å where tube sensitivity is low and where the calibration is uncertain because of atmospheric absorption and the blue leak of the grating. At the region close to atmospheric cutoff $\lambda \lesssim 3300$ Å, low counting statistics and unknown atmospheric transmission variations also lead to lower photometric accuracy.

The relative line fluxes for the objects observed are given in Table 1. For those objects in common with Brugel, Böhm, and Mannery (1981*b*), who used the multichannel scanner on the Mount Palomar 5.08 m telescope and the image dissector scanner on the Kitt Peak 2.13 m telescope, the agreement with the strong lines is excellent. For the weaker lines, our spectrophotometry tends to give systematically higher relative intensities. We believe this to be caused by the presence of many faint lines, mainly of Fe II which at inferior resolution to ours would blend to form a quasi-

TABLE 1—*Continued*

		HH 2H		HH 3		HH 43		HH 47		HH 47 Bridge	
Ident.	λ (Å)	F	F_o	F	F_o	F	F_o	F	F_o	F	F_o
[OII]	3727,9	148.2	222	324	372	96.2	118.2	81.3	87.1	173.3	213
H10	3797,9	2.94	4.3	-	-	3.4	4.1	-	-	-	-
H9	3835,4	4.6	6.6	6.6	7.5	5.1	6.1	-	-	7.1	8.5
H8, HeI, [NeIII]	3868	16.7	23.7	10	11.3	-	-	-	-	6.2	7.4
Hε, HeI	3889	11.5	16.2	8.8	9.9	7.8	9.3	7.4	7.8	13.2	15.7
CaII	3934	12.6	17.7	13.0	14.5	7.8	9.2	44.1	46.6	23.2	27.4
CaII, [NeIII]	3968	25.7	35.1	24.6	27.3	13.4	15.7	48.5	51.1	22.7	26.6
[SII]	4068,76	53.1	70.0	32.3	35.5	61.3	70.5	77.3	81.0	18.4	21.2
Hδ	4100	19.9	25.9	20.3	22.2	15.4	17.6	19.5	20.4	22.6	25.8
[FeII]	4245	5.9	7.3	6.8	7.3	2.7	3.0	15.1	15.6	6.7	7.5
[FeII]	4276,87	6.9	8.4	9.0	9.6	4.6	5.1	26.6	27.5	9.9	11.0
Hγ	4340	38.3	45.8	43.3	46.0	37.2	40.7	42.4	43.7	42.3	46.3
[OIII], FeII	4363	12.4	14.7	7.8	8.3	5.6	6.1	5.2	5.3	-	-
[FeII]	4415	7.2	8.4	7.7	8.1	3.7	4.0	16.7	17.1	-	-
[MgI], FeII	4562,71	3.7	4.1	10.0	10.3	14.5	15.3	38.3	39.0	18.7	19.7
HeII	4686	8.0	8.5	-	-	-	-	-	-	-	-
Hβ	4861	100		100		100		100		100	
[OIII]	4959	30.2	29.3	11.3	11.2	1.7	1.7	-	-	-	-
[OIII]	5007	85.0	81.4	36.7	36.2	5.6	5.5	< 1.0	< 1.0	7.0	6.8
[FeII]	5158	21.3	19.4	16.1	15.6	7.5	7.2	38.6	39.2	9.5	9.9
[NI]	5198,20	11.8	10.6	25.8	24.9	120.6	114.2	129.3	127.0	60.1	56.9
[FeII]	5261,73	17.8	15.7	8.3	7.9	3.2	3.0	20.3	19.9	6.7	7.1
[FeII]	5334	4.7	4.0	2.1	2.0	-	-	4.0	3.9	-	-
[FeII]	5528	4.9	4.0	2.4	2.6	2.3	-	-	-	-	-
[NII]	5755	8.8	6.8	-	-	3.3	2.9	-	-	-	-
HeI	5877	8.8	6.6	4.2	3.8	-	-	-	-	-	-
[OI]	6300	202	138	121	106	452.5	373	342	320	127.5	105
[OI]	6364	75.3	50.1	39	34.0	147.3	119.7	108.6	101.4	31.7	25.7
[NII]	6548	74	47.4	36.9	31.7	37.2	29.6	27.7	25.7	22.0	17.5
Hα	6563	538	342.7	424.7	364	575	457.1	500	463.2	401.7	319.4
[NII]	6583	287	182.1	165.7	142	120.6	95.7	72.5	67.1	64.3	51.0
HeI	6678	2.5	1.6	-	-	-	-	-	-	-	-
[SII]	6717	70.2	43.3	141.7	120.3	464.8	363.7	486.2	488	197.5	154.5
[SII]	6731	138.2	85.1	139.9	118.7	450.6	352.1	511	471	152.0	118.8
HeI	7065	-	-	-	-	-	-	-	-	-	-
[FeII]	7155	51.7	29.6	16.0	13.2	7.0	5.3	32	29	-	-
[FeII]	7172	10.0	5.7	-	-	-	-	14	12.7	9	6.8
[CaII]	7291	50.3	28.2	26.5	21.8	19.4	14.4	125	113	35.3	26.3
[OII], [FeII]	7318,30	173	96.3	45.4	37.2	18.4	13.6	71	64	35.5	26.3
FeII, NiII	7376	25	13.8	13.2	10.8	-	-	32	29	10	7.4
$C_{S,O}$		0.586		0.198		0.295		<0.18		<0.35	
C_{Bal}		0.665		0.377		0.822		0.62		0.34	
C_{adopt}		0.59		0.2		0.3		0.1		0.3	

continuum. This would certainly be true for multichannel scanner observations, and the very extended wings of the IDS instrumental response function would also tend to militate against detection of very faint lines in such a rich spectrum. To give some idea of the magnitude of the problem, we show in Figure 1 our reduced spectrum of HH 2H, scaled to show the continuum. On this scale, the peak of the Hβ is 10 times higher than the upper boundary of the plot. Clearly, between 3600 and 5600 Å very few points are representative of the continuum. We have indicated on the plot the actual continuum wavebands used, with their nominal central wavelengths, which vary in width from 30 to 110 Å. We make no attempt to list and classify all the faint emission lines and blends, as unambiguous identifications clearly require higher resolution.

Despite our better resolution, Figure 1 suggests that there may still be some blending problem in measuring the continuum near the Balmer jump. Since the faint lines are due principally to [Fe I] and [Fe II], the possible number of faint lines that can contaminate the measures can be estimated from Moore's (1945) multiplet tables. For example, the 4170 Å band has 19 lines, the 3600 Å band four (all of which would be resolvable), the 3500 Å

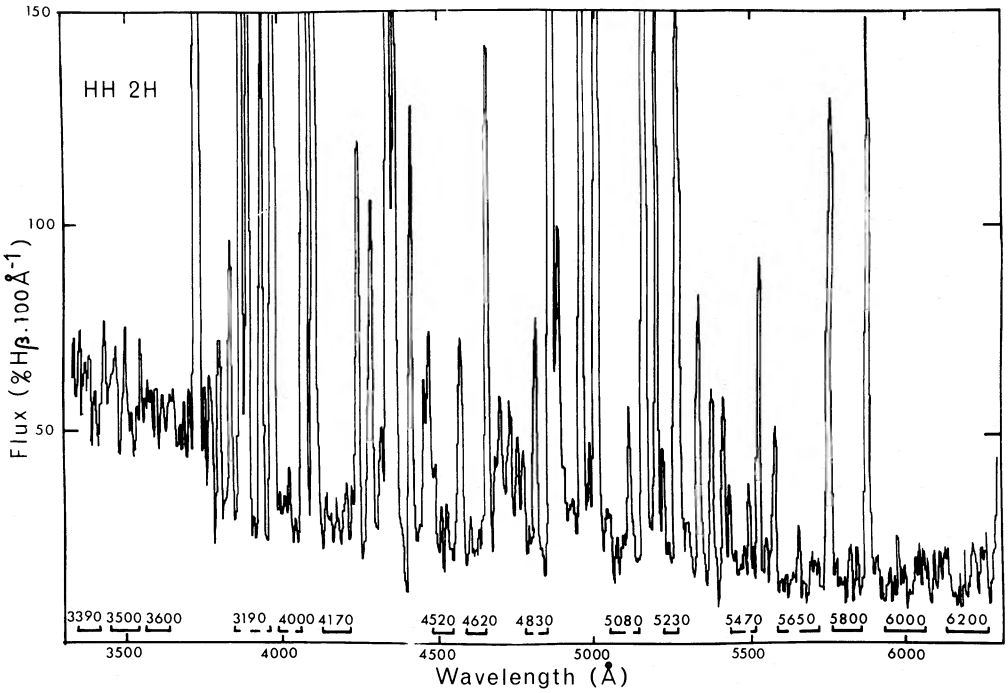

FIG. 1.—The reduced observations of HH 2H scaled to show the continuum. The actual "continuum" bands used are shown at the bottom with their nominal wavelengths.

band 20, and the 3390 Å band six. Thus the principal effect of blends would be to produce a systematic enhancement of some continuum bands with respect to others, an effect which is not seen in our results. In any event, the contribution of the forbidden iron lines is most important for the dense, high excitation HH objects, whereas it is the low-density, low-excitation objects which show the strongest continuum. In terms of signal strength, the continuum from the various HH objects is detected at or above the 10 σ level for $\lambda < 4000$ Å, falling to the 3 σ to 5 σ level near $\lambda = 6000$ Å. We thus conclude that both our resolution and sensitivity are indeed sufficient to measure the true continuum.

We find that the present spectrophotometry, and that of Böhm, Schwartz, and Siegmund (1974) and Brugel, Böhm, and Mannery (1981*b*) agrees very poorly with that of Dopita (1978). The latter shows much greater intensities for red lines, except in the case of HH 47 which was observed separately from the rest. We can only conclude that some undetected calibration problem affected the earlier IDS work. The present work should therefore be considered as superseding those already published. In any event, the reddening correction procedure used in the earlier work gives too low values, and this will also lead to an overestimate of the intrinsic Balmer decrement.

III. CORRECTIONS FOR REDDENING

With their large wavelength base, Brugel, Böhm, and Mannery (1981*b*) were able to apply Miller's (1968) method to determine the amount of interstellar extinction. This consists of comparing the relative intensities of the 4068, 4076 Å with the 10,318, 10,336 Å lines of [S II]. Since these arise from common upper levels, the theoretical relative intensities depend only on the transition probabilities.

Dopita (1978) used the theoretical ratio of the 4069, 4076 Å to the red 6717, 6731 Å lines of [S II] as a function of the density sensitive 6717/6731 Å line ratio as derived from shock models. This will work only if the models are accurate and if they are a true representation of the physical conditions in the HH object. This latter assumption is questionable, as the spectra of many HH objects do not fit well to steady-flow shock models.

We propose here a new technique which overcomes the above objections and should give a reasonably reliable value for the extinction correction independent of the hydrogen lines, when spectrophotometry of limited baseline is all that is available. Consider the ratio R which is a product of the ratios of the red to blue lines of [S II] and [O II], viz.,

$$R = \left(\frac{6717, 6731}{4068, 4076}\right) \cdot \left(\frac{7318, 7328}{3727, 3729}\right).$$

Since the red lines of sulfur and the blue lines of oxygen arise in transitions from the ^2D states of p^3 ions, these will both be subject to some collisional de-excitation at high ($n_e \gtrsim 10^2$ cm^{-3}) densities. The density dependence will tend to be minimized by the division of one pair by another. The blue [S II] lines and the red [O II] lines, on the other hand, arise from transitions out of the upper ^2P metastable levels. Thus, much of the temperature dependence of the red to blue line ratios

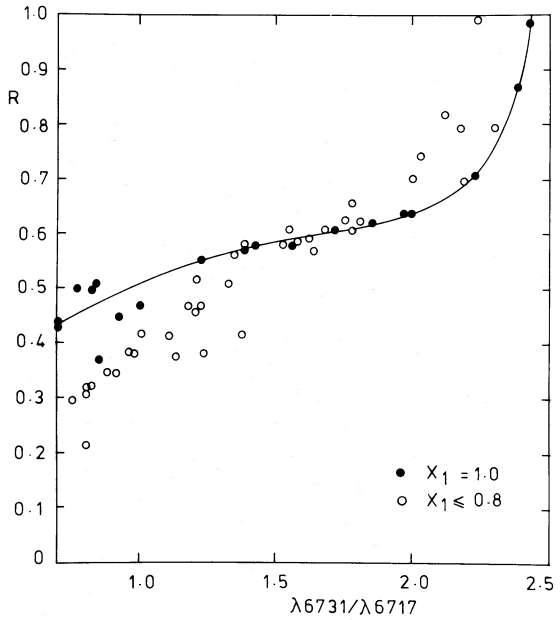

FIG. 2.—The dependence of the reddening sensitive ratio R (defined in the text) as a function of electron density implied by the [S II] ratio. Many models of differing initial parameters are shown. Models with hydrogen preionization fraction, x_1, of less than 0.8 are shown as open circles.

for each species is removed by the formation of the ratio R. It is easy to show that at electron temperature T, the remaining temperature dependence in R is exp $[\Delta E/kT]$, where ΔE is the difference between the ^2P–^2D energy gaps of the S II and O II ions. This is exp $[-5750/T]$ putting in numbers, and is therefore weak at normal temperatures encountered in emission nebulosities, assuming the two species arise from regions with similar temperatures.

We have investigated the residual density dependence in the case of shock models by computing a large number of plane-parallel radiating shocks of various preionizations using a new and improved modeling code MAPPINGS developed by Binette and Dopita at Mount Stromlo which is also capable of modeling photoionized nebulosities of all types and shocks which have ionization structure consistent with their internal production of ionizing photons, or with external sources of photons. In Figure 2 we show the results of a large variety of shock models with different velocities, preionizations, initial magnetic fields, preshock densities, and shock ages. The ratio R gives us a reliable function of density up to [S II] $\lambda6731/\lambda6717$ ratios of order 2.1 ($n_e \lesssim 1.5 \times 10^4$ cm^{-3}; Pradham 1976). The solid line connects a family of fully steady flow shock models with full preionization and varying shock velocity and density (zero magnetic field). The factor which contributes most severely to scatter on the figure is the preionization, which presumably acts through the residual temperature sensitivity discussed above by altering the temperature and ionization structure of the shock. The mean scatter of $\sim 20\%$ in R at a given density indicated by the [S II] lines is not very important since this will contribute only 14% error to the logarithmic reddening constant or 12% in terms of $E(B-V)$. A more serious correction in the present context is the influence of the [Ca II] line on the measured $\lambda7318$, 7328 [O II] intensities. We have assumed that the [Ca II] $\lambda7324$ has an intensity of two-thirds of the [Ca II] 7291 Å line in order to deblend the [O II] doublet. In Table 1, the reddening constants, C_{SO}, derived from the ratio R are given, along with the constant, C_{Bal}, determined from the Balmer lines of hydrogen. To form this latter quantity, the observed Hγ/Hβ and Hδ/Hβ ratios are given double weight, higher members of the series to Hβ are given single weight because of the lower signal to noise, and the Hα/Hβ ratio is given single weight to allow for the probability that Hα is affected by collisional excitation. The two values of reddening constant so derived agree very well in HH 1, 2, and 3, with no obvious tendency for C_{Bal} to be systematically larger than C_{SO}. We have adopted a mean reddening constant from all measurements in HH 1 and 2 to derive extinction corrected line and continuum flux. These are 0.76 and 0.59, respectively, and are in excellent accord with the values of 0.724 and 0.591 obtained by Brugel, Böhm, and Mannery (1981*b*) for these same objects.

IV. THE CONTINUUM OBSERVATIONS

The continuum was estimated as the mean flux within the bands marked in Figure 1 and has been expressed as a percentage of the flux of Hβ per 100 Å in Table 2. These are then corrected for reddening as described above.

Inspection of the table shows that the Balmer discontinuity is present in all objects with about the same relative intensity. This is made more evident in Figures 3 and 4, where the reddening corrected observations with their estimated errors due to statistics alone are plotted in order of increasing "blue excess" judged from the strength of the continuum in the 3390 Å band. Thus, whatever is causing the excess is largely independent of the bound-free recombination continuum. The ratio of the Balmer discontinuity to Hβ can be used to estimate the recombination temperature. These temperatures are given in Table 3 and are derived using effective recombination coefficients given by Brown and Mathews (1970) and Brocklehurst (1971) and, because of the relatively weak temperature dependence, are only accurate to about ± 2000 K. We also include the Hα/Hβ ratio and the [O I]/[O III] (6300/5007) ratio after correction for reddening.

Two factors are worthy of note. First, the recombination temperatures are much higher than those expected for a steady flow shock, which would give (from our models) a temperature in the range 6000–8000 K. Second, there is a weak, but real, correlation between the recombination temperature, the Hα/Hβ ratio, and the amount of neutral matter in the radiating zone judged by the [O I]/[O III] ratio. We return to this point in § V.

TABLE 2

OBSERVED AND REDDENING CORRECTED CONTINUUM FLUXES

	HH 1 NW		HH 1 SE		HH 2A		HH 2B		HH 2G		HH 2H		HH 3		HH 43		HH 47		HH 47 Bridge	
λ (Å)	F	F_0	F	F_0	F	F_0	F	F_0	F	F_0	F	F_0	F	F_0	F	F_0	F	F_0	F	F_0
3390	50.1	97.9	87.4	170	43.9	74.3	55.4	93.7	63.9	108	60.1	102	74.2	88.5	133	174	173	189	130.1	170
3500	51.8	96.1	75.3	140	42.7	69.3	49.2	79.9	63.4	103	58.2	94.5	71.5	84.3	117	150	138	150	121.8	156
3600	54.7	96.9	79.9	142	40.0	62.6	50.6	70.2	62.7	98.1	57.6	90.2	74.2	86.4	108	136	149	161	112.3	141
3910	24.8	38.6	54.2	84.3	18.4	26.0	23.8	33.7	34.9	49.4	29.0	41.0	35.7	40.2	78.1	93	88	93	61.7	74
4000	31.1	45.5	49.7	72.7	19.7	26.5	23.1	31.1	34.3	46.2	30.1	40.5	33.1	36.6	72.5	84	98	103	55.8	65
4170	25.3	34.2	52.7	71.2	18.3	23.2	22.9	29.0	35.4	44.8	29.1	36.8	28.4	30.8	65.4	73.8	77	80	52.2	59
4520	25.3	29.6	54.2	63.3	14.4	16.3	19.3	21.8	27.9	31.5	25.3	28.6	21.8	22.7	56.7	60.3	66	67	45.7	48.6
4620	26.5	29.4	46.7	51.9	15.1	16.4	16.4	17.8	29.1	31.6	23.5	25.5	20.3	20.9	50.5	52.7	64	65	49.3	51.4
4830	24.2	24.5	43.6	44.2	13.9	14.1	17.4	17.6	24.9	25.2	21.6	21.8	19.9	20.0	48.9	49.2	60	60	47.1	47.4
5080	22.4	20.5	48.2	44.2	13.0	12.1	15.3	14.3	22.4	20.9	19.7	18.4	15.7	15.3	48.1	46.5	54	53	43.5	42.0
5230	20.6	18.5	48.2	43.4	10.7	9.9	16.9	15.6	22.4	20.6	19.7	18.1	14.2	13.8	44.1	42.3	44	43	41.7	40.0
5470	19.4	15.3	49.6	39.2	11.2	9.3	13.7	11.4	19.6	16.3	18.6	15.5	11.5	10.8	35.5	32.3	36	35	32.6	29.7
5650	17.7	13.1	43.6	32.3	10.0	7.9	12.6	10.0	16.0	12.7	15.4	12.2	11.5	10.8	33.9	30.1	30	29	36.2	32.1
5800	17.1	11.7	42.2	28.9	9.7	7.2	12.0	8.9	15.3	11.4	14.6	10.8	12.8	11.6	32.3	27.7	26	25	37.0	31.8
6000	15.3	10.1	40.7	27.0	9.7	7.0	9.6	6.9	15.9	11.5	15.5	11.2	11.5	10.3	32.3	27.4	27	25	34.0	28.8
6200	16.4	10.2	49.7	31.0	10.2	7.0	14.4	9.9	18.9	13.1	17.2	11.9	12.0	10.6	30.8	37.2	22	21	37.6	31.1

NOTE.—Fluxes given as % Hβ flux per 100 Å.

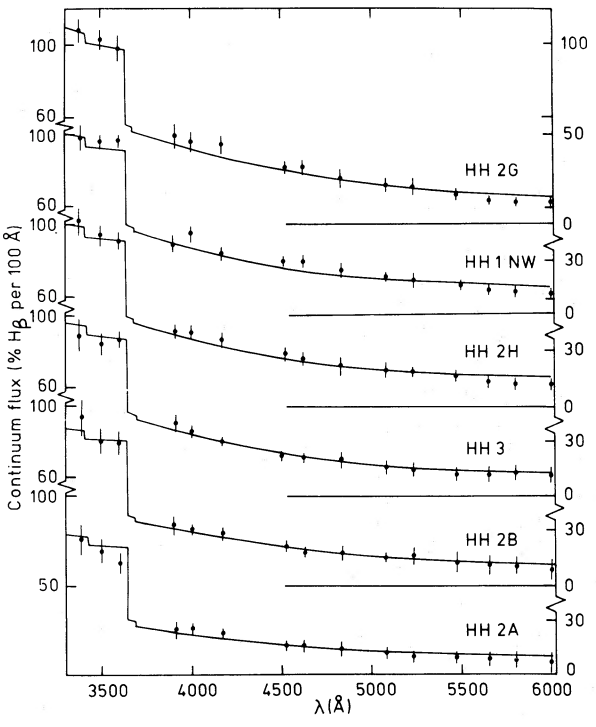

FIG. 3

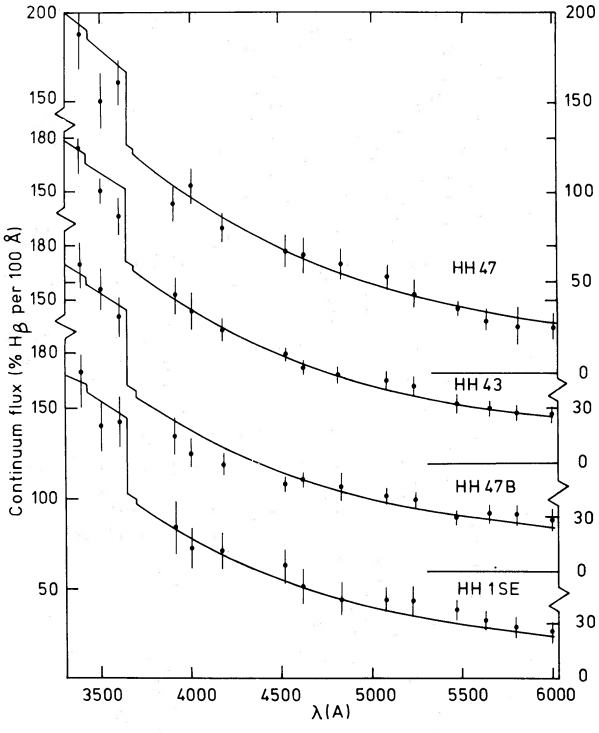

FIG. 4

FIG. 3.—The observed continuum intensity in HH objects, corrected for reddening compared with a variable two-photon continuum plus 10,000 K bound-free and free-free model (*solid line*).

FIG. 4.—As in Fig. 3

TABLE 3

TWO-PHOTON ENHANCEMENT FACTORS IN HH OBJECTS

Object	$\langle T_{rec} \rangle$	f_{2q}	Hα/Hβ	[O I]/[O III]
HH 1 SE	17,000	10.6	3.4	7.1
HH 1 NW	8500	5.5	3.0	2.6
HH 2A	15,000	2.8	3.3	0.6
HH 2B	10,000	4.3	3.3	2.3
HH 2G	10,000	6.2	3.1	3.9
HH 2H	10,000	5.4	3.4	1.7
HH 3	14,000	4.8	3.6	2.9
HH 43	20,000	11.3	4.6	21.8
HH 47B	10,000	11.7	3.2	15.4
HH 47	16,000	13.3	4.6	>320

NOTE.—HH 47B refers to the bridge of high-velocity nebulosity connecting HH 46 with HH 47.

V. INTERPRETATION

a) *The Two-Photon Continuum*

The observations of Brugel, Böhm, and Mannery (1981*a*) have shown that the continuum of HH objects could be approximated by a power law spectrum $F_\lambda \propto \lambda^{-n}$ with $2 \lesssim n \lesssim 3$, and we know that this blue continuum continues to rise into the far-UV (Ortolani and D'Odorico 1980; Böhm, Böhm-Vitense, and Brugel 1981). We have shown above that at least a portion of this continuum is due to bound-free Paschen and Balmer continua and is intrinsic to the HH object. We would like to assume that the rest of the continuum is also intrinsic to the source—an assumption strongly suggested by the fact that the intensity of the continuum is very highly correlated with the intensity of the Balmer lines across individual HH knots in our spectra. If this is the case, what process could give rise to a blue continuum? We propose here that a collisionally excited two photon ($2q$) continuum of hydrogen is the cause. In the 3000–6000 Å range this follows a power law nearly exactly with exponent n, as defined above, equal to 3.3. This operates in the opposite sense to the bound-free Paschen continuum of hydrogen, which has an exponent of roughly -1.1 in the same wavelength range. Thus, as noted by Dopita (1981), an admixture of the two processes could produce a wavelength dependence of the continuum intensity in the range observed by Brugel, Böhm, and Mannery (1981*a*). Although the $2q$ continuum is generally thought of as a relatively minor contributor to visible recombination continuum spectra (Brown and Mathews 1970), the collisional enhancement of this process has already been noted in shocked plasmas from UV observations of the Cygnus Loop (Benvenuti *et al.* 1980), where it is enhanced by roughly a factor 2 over the recombination value. To explain the present observations, much larger enhancements are required.

Figures 3 and 4 show the observations and theoretical continua fitted to each object (*solid lines*). The curve fitting procedure was simply to add an arbitrarily large theoretical two-photon distribution (the intensity of which was estimated primarily from the 3910, 4000, and 4170 Å measured points) to a theoretical bound-free recombination spectrum of hydrogen and helium, assuming a helium abundance of 0.1 by number. The recombination temperature was kept fixed at 10^4 K for all the fits to reduce the number of independent variables to one, the relative intensity of the $2q$ continuum. Considering the simplicity of this procedure, and the range over which the $2q$ intensity ranges, we find the fit of theory and observation to be remarkably good, proving that the spectral distribution of the continuum is consistent with our hypothesis.

Using the computed recombination temperatures in Table 3, we have computed the factor, f_{2q}, by which the $2q$ continuum is enhanced over its recombination value. These range up to 13.3 which implies a total flux in the continuum as large as 145 times the flux emitted in Hβ!

The $2q$ excess is weakly correlated with the recombination temperature and the Hα/Hβ ratio, but shows a very close correlation with excitation class of the HH spectrum in the sense that low-excitation objects show large $2q$ excesses. To illustrate this, we have formed two excitation parameters: the [O I] λ6300/[O III] λ5007 ratio mentioned above, and a mixed ratio which is the product of the [N I] λ5198, 200 and [O I] 6300 Å lines divided by the product of the [N II] 6584 Å and the [O II] 3727, 3729 Å lines. We plot f_{2q} as a function of these two ratios in Figures 5 and 6. Of these the former is likely to be more sensitive at high shock velocities whereas the latter will be better at lower velocities. Not only are the two correlations excellent, but the point for the Cygnus Loop (Benvenuti *et al.* 1980) falls on the continuation of the trend to higher excitation class.

b) *Theoretical Models*

The most probable source of the $2q$ enhancement is the collisional excitation of hydrogen in shock waves propagating through a gas which is predominantly unionized. Steady-flow models have not in the past satisfactorily reproduced the observed spectral signature

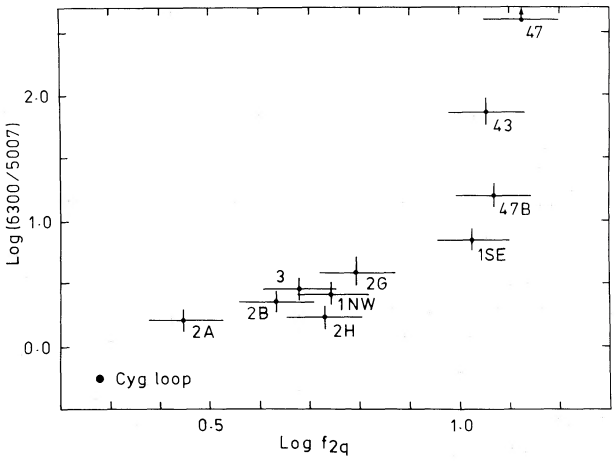

FIG. 5.—The enhancement factor of the two-photon continuum, f_{2q}, as a function of excitation measured by the [O I]/[O III] ratio.

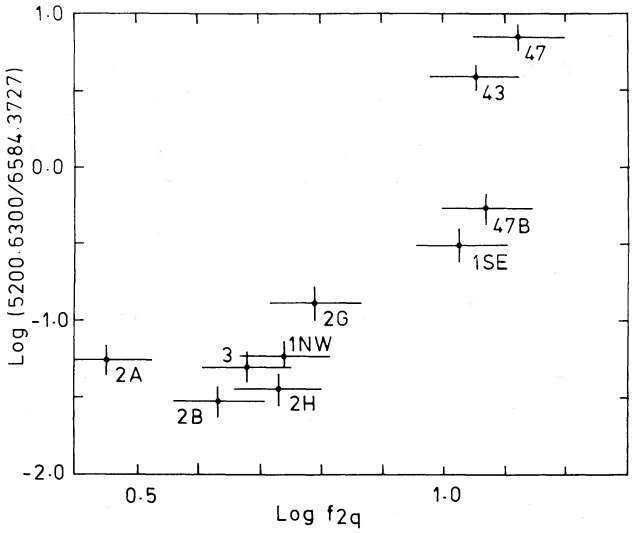

FIG. 6.—The enhancement factor of the two-photon continuum, f_{2q}, as a function of the excitation given by the [O I] × [N I]/[O II] × [N II] ratio.

of those low-excitation HH objects which lie in this regime (Dopita 1978). We have substantially modified the earlier shock modeling code used previously to include a much more complete account of the physical processes at work, including the important charge-exchange reactions. The code (program MAPPINGS, mentioned in § III) incorporates 12 elements with up to six ionization stages each. Sixteen ions of the p^2 and p^3 configuration are solved as five-level atoms for their forbidden lines. The code includes 48 intercombination lines and 59 resonance lines. For the resonance lines, including H I, He I, and He II lines, the collisional excitation is solved allowing for the temperature dependence of the gaunt factors. The Balmer lines to Hβ and the intensity of the two-photon continuum are computed, allowing for both collisional excitation and recombination cascade. For hydrogen and the resonance lines, neither case A nor case B is explicitly assumed, since shocks tend to be closer to case A at the high temperature end but approximate to case B near the recombination zone. We solve the radiative transfer of these lines using a Capriotti (1965) escape probability formulation to approximate the diffusion up and down the shock. For UV resonance lines able to ionize hydrogen, the higher photon density within a zone of a shock implied by a low escape probability per scattering enables a larger fraction of these photons to be absorbed *in situ* by photoionization. Thus our models tend to have lower self-consistent preionization fractions for a given velocity than those of Shull and McKee (1979) who did not take this effect into account. However, in the modeling of HH shocks, the velocities are generally so low that shock self-preionization is negligible and essentially identical results are obtained by neglecting the internal photionizing fields entirely.

A much more important problem concerns the computation of the Balmer decrements. Although the recombination and cascade problem is well defined (Pengelly and Seaton 1964; Brocklehurst 1971) the collisional excitation rates for hydrogen are less so, particularly for the Lyβ transition which determines the collisional contribution to the Hα intensity. Osterbrock (1974) recommends use of the Burke, Ormonde, and Whitaker (1967) threshold cross section which is computed theoretically using multistate close-coupling theory. However, as these authors note interstate coupling may not be fully accounted for. The experimental measurements of Kleinpoppen and Kraiss (1967) show evidence for a complex resonance structure just above threshold, and we find that using the Burke, Ormonde, and Whitaker (1967) computations to normalize the experimental data, these do not converge to the Born approximation at high energy, but lie approximately 3.5 times higher. We have therefore adopted the Johnson (1972) rates for collisional excitation for all levels, except that we have adjusted this in the case of the $n = 1 \rightarrow 3$ transition to account for the experimentally measured resonance structure. This is important in the regime $T_e \lesssim 100{,}000$ K.

In all our models, the abundances of the heavy elements (by number) was fixed in the solar proportions, namely H:He:C:N:O:Ne:Mg:Si:S:Cl:Ar as

$$1.0{:}0.1{:}3.3 \times 10^{-4}{:}9.1 \times 10^{-5}{:}6.6 \times 10^{-4}{:}8.3 \times 10^{-5}{:}$$
$$2.6 \times 10^{-5}{:}3.3 \times 10^{-5}{:}1.6 \times 10^{-5}{:}$$
$$4 \times 10^{-7}{:}6.3 \times 10^{-6}\,.$$

Models with low preionization have quite a different structure from fully preionized computations. This is illustrated in Figure 7, which is the detailed model on which Table 4 is based. The shock velocity is 34.7 km

TABLE 4

COMPARISON OF A LOW-EXCITATION SHOCK MODEL OF FINITE AGE WITH TWO HH OBJECTS

Ion	λ	Model[a]	HH 43	HH 47
[O II]	3727, 9	269	118	87
[S II]	4068, 76	66.9	70.5	81
Hδ	4100	18.8	17.6	20.4
Hγ	4340	39.0	40.7	43.7
Hβ	4861	100	100	100
[O III]	5007	<0.1	1.7	<0.5
[N I]	5199	171	114	127
[O I]	6300	535	373	320
[O I]	6363	166	120	101
[N II]	6548	11.2	29	26
H	6563	432	457	463
[N II]	6584	33.0	95	67
[S II]	6717	406	363	448
[S II]	6731	366	352	471
[O II]	7318, 30	6.8	4	<10
$\log (F_{2q})$	...	1.00	1.05	1.12
$\log \frac{5199.6300}{6584.3727}$	...	1.01	0.66	0.84

[a] Model parameters: $V_s = 34.7$ km s^{-1}, $N_1 = 500$ cm^{-3}, $B_1 = 50$ microgauss, $X_1 = 0.1$, $\tau_s = 30$ years.

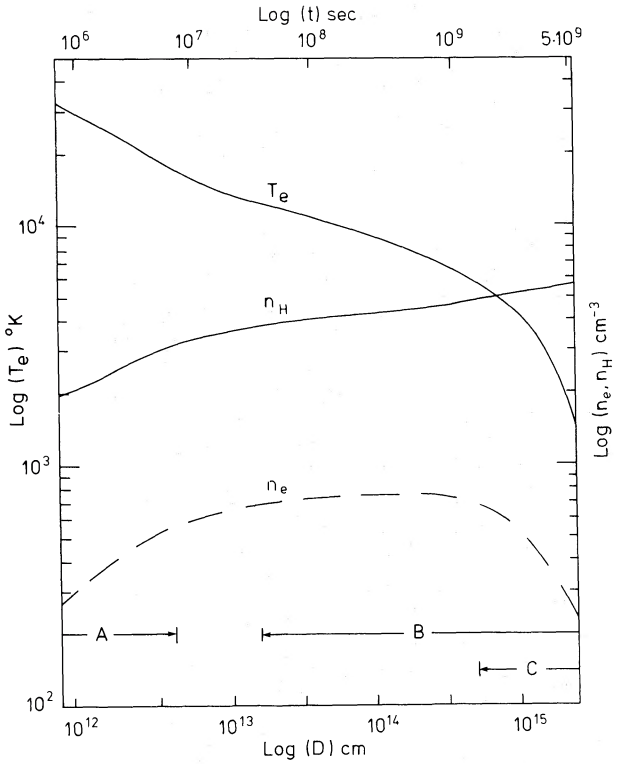

FIG. 7.—The structure of a shock model with 0.1 fractional preionization. D is the distance from the shock front, t the time, and T_e, n_e, and n_H refer to the electron temperature, electron density, and hydrogen number densities, respectively. The full shock parameters are given in Table 4.

s^{-1}, and fractional preionization x is 0.1, giving a postshock temperature of 40,000 K.

The structure can be roughly divided into three zones marked A, B, and C on Figure 7, although their boundaries are somewhat ill defined. The initial cooling, A, is exceedingly rapid and is dominated by collisional excitation and, to a lesser extent, collisional ionization of hydrogen. This lasts less than a year in this model. Although the layer of gas is very thin, it is this region that accounts for the majority of the total cooling and in which the large two-photon excess is produced, although the contribution to the Balmer lines is very small.

In region B, most of the cooling is through collisional excitation of forbidden lines. Hydrogen starts to recombine, giving a normal recombination-cascade spectrum. In this model, recombination is 91% complete after 10^{10} s, when the temperature is 100 K. Because of the high initial transverse magnetic field of 50 microgauss, this model is dominated by magnetic field pressure in region C, and as a result a large decrease in temperature is accompanied by only a small increase in particle density. This region would reexpand if the pressure driving the shock were only of an impulsive nature.

By systematically varying the shock velocity and preshock ionization, we find a rather tight relationship between the Hα/Hβ relative flux and the intensity of the two-photon continuum. Because of the dominance of two-photon emission in region A of the shock, of the two parameters the preionization is the most important in determining the correlation. In Figure 8 we show a family of models with fixed postshock temperature and varying preionization as a solid line (curves of other postshock temperatures lie close). Note that even at very low values of preionization the Balmer decrement and the $2q$ lie below that observed in HH 43 or HH 47. The models also fail to reproduce the forbidden line excitation. In Figure 9 we plot the same family of models on a diagram similar to Figure 6.

However, an excellent description of the spectral signatures of the low-excitation HH objects can be obtained by shocks of finite age, produced by the simple expedient of sawing off the theoretical model before the

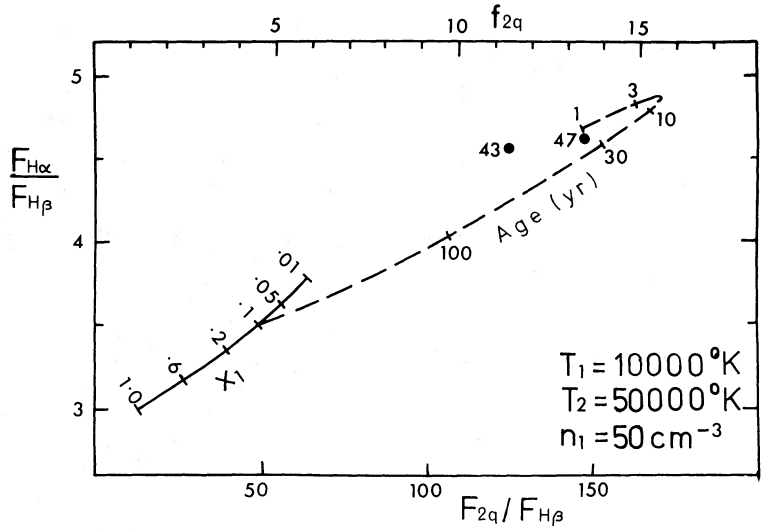

FIG. 8.—The theoretical relationship between two-photon excess and Balmer decrement for a family of shock models with differing preionization (x_1) and age. The observed positions of HH 43 and HH 47 are also shown.

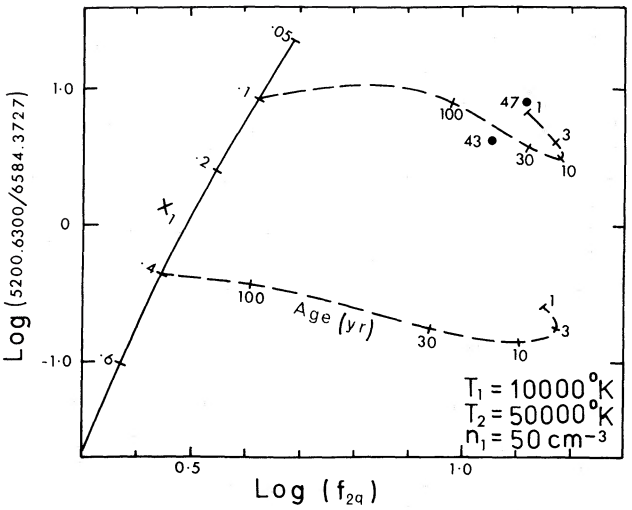

FIG. 9.—The theoretical relationship between two-photon excess and the excitation parameter of Fig. 6 for a family of shocks of differing preionization, x_1, and age. The observed positions of HH 43 and HH 47 are also shown.

gas has fully cooled and recombined. Trajectories of age are shown in Figures 8 and 9 for fixed shock conditions. Agreement on $2q$ strength, Balmer decrement, excitation level, and absolute strength of the forbidden lines with respect to Hβ is obtained in the vicinity $\tau \sim 50$ years. Table 4 shows a higher density model with a reasonable magnetic field, which is in better agreement with the [S II] density sensitive line ratios in HH 43 and 47. The fit of the model with the observations is as good as could be hoped for. However, the computed age is unexpectedly short compared with the dynamical evolution time scale, and the computed shock velocity is much lower than the radial velocity measured for these objects.

Thus the conclusions of Schwartz and Dopita (1980) and Böhm, Brugel, and Mannery (1980) that the preshocked material already has a substantial space velocity when it is reshocked is confirmed. Schwartz and Dopita (1980) developed a model in which the HH objects represent cloudlets which have been steadily accelerated by a stellar wind. Although a steady mass loss of order $10^{-5}\ M_\odot\ \mathrm{yr}^{-1}$ was implied, there is increasing evidence to support the idea that the wind from the central star is focused by density gradients (Cantó 1980; Cantó and Rodriguez 1980; Barral and Cantó 1981) which reduces the steady mass-loss requirements to the order of $10^{-7}\ M_\odot\ \mathrm{yr}^{-1}$.

However, our model has such a low age that a hypothesis of episodic mass loss now appears preferable. A consequence of this would be that each cloudlet is repeatedly shocked as it is accelerated toward the terminal velocity of the stellar wind. Since each shock tends to amplify the importance of magnetic pressure with respect to the gas pressure by compression of the transverse component and possibly by turbulence in the cooling region, clouds that have been multiply-shocked probably derive most of their pressure support from magnetic fields. To test this we ran a model with a preshock density of 2000 cm^{-3} and a transverse magnetic field of 1000 microgauss, and obtained a spectrum very similar to the model of Table 4. If the pressure pulse driving the shock declined on a characteristic time scale of ~ 30 years, then the magnetic-field overpressure would cause the gas to reexpand, thus inhibiting recombination and lowering the emission measure in the recombination zone. This would cause the shock spectrum to look like a 30 year old shock even though the shock might have been propagating for longer time scales.

VI. CONCLUSIONS

We find that an enhanced $2q$ continuum plus recombination continua is sufficient to describe the continuum distribution of all HH objects we observed. The strength of the $2q$ component is anticorrelated with the excitation of the nebula and directly correlated with the intrinsic (reddening corrected) Balmer decrement. These facts argue strongly against an extrinsic source for the continuum. This conclusion differs from that of Ortolani and D'Odorico (1980) and Brugel, Böhm, and Mannery (1981*a*). Those authors argued against the $2q$ interpretation on the grounds of the absolute strength of the continuum in the far-ultraviolet and the fact that it shows no clear tendency to decrease shortward of 1450 Å. With the $2q$ enhancement we have shown to be possible in collisionally excited gas, the first of these objections can be surmounted. Within the uncertainties of calibration of the optical and UV data, our observed $2q$ excess in HH 1 NW would fit well to the observed flux in the 1500 Å region. Neither do we believe that the lack of a well defined turn-down below 1450 Å is a serious problem. The signal-to-noise ratio judged from Figure 1 of Brugel, Böhm, and Mannery's (1981*a*) paper, is only around 2:1. Furthermore, in view of the observed strength of the O I λ1306 line, we might also expect C I $\lambda\lambda$1262, 1278, and 1330 lines and the O I] λ1356 line to contribute to the blending problem in this region. When one also takes into account the fact that the sensitivity of the *IUE* system is declining rapidly over the same range, it seems clear that measurements of higher sensitivity are required to settle the question.

Brugel, Böhm, and Mannery (1981) have argued convincingly that the blue-UV continuum cannot be due to scattered light from a T Tauri star. The only alternative to the enhanced $2q$ hypothesis would be to associate a hot ($T \approx 40{,}000$ K), subluminous star with each HH object. To the extent that the continuum is coextensive with the nebula, the stellar radiation would have to be scattered outward by dust which is coextensive with the nebula. There is no visible, IR, or radio evidence for the existence of stellar components coincident with HH objects or for the compact H II regions that such hot objects would produce.

Herbig and Jones (1981) have shown that the proper motions of HH1 and HH2 implicate a faint extremely reddened T Tauri star lying between them as the source of energy. Both objects appear to have been generated in or by material ejected from the star, supporting the

idea of excitation by a focused stellar wind discussed in the previous section. The velocity of this wind must be very high to allow the velocities of some 200 km s^{-1} seen in some HH objects. The soft X-ray emission detected by Pravdo and Marshall (1981) therefore could be due to a bow shock in the stellar wind around the HH cloudlet. A stellar wind of 300 km s^{-1} will produce post shock temperatures in excess of 10^6 K. However, the association of the X-ray source with HH 1 is not unambiguous.

The theoretical shock wave models which most closely describe the observation of the low-excitation HH objects are those with partial preionization, finite age, and, possibly, very large magnetic fields in the preshock region. This argues for a variable or pulsed stellar wind as the source of the excitation. Certainly a good case for high activity in the central star can be made for HH 46 and 47. A spectrum of HH 46 shows the stellar object and the surrounding nebula to be a very luminous T Tauri star with continuous spectrum and very strong [O I], [Fe II], and Balmer emission almost identical in spectrum with DG Tau observed by Cohen and Kuhi (1979). These authors have shown that bolometric luminosity is correlated with the chromospheric activity in T Tauri stars as measured by the emission lines, and certainly the presence of [O I] λ6300 and the relative weakness of the 5577 Å feature proves the existence of an extended low density ($n_e \lesssim 10^4$ cm^{-3}) envelope. Eruptive activity may be the link between T Tauri stars and the FU Orionis phenomenon. Cantó *et al.* (1981) claim an association between R Mon, NGC 2261 (its reflection nebula), and HH 39 on the basis of the directed stellar wind model (Cantó 1980; Barral and Cantó 1981). Imhoff and Mendoza (1974) estimated a luminosity of 660 $L_\odot$ and spectral type A5 I for R Mon. However, it has brightened considerably since Joy (1945) classified it as a Ge T Tauri variable. Among the three objects classified in the FU Orionis class, one (V1057 Cygni) was known to be a T Tauri star before outburst.

Larson (1980) has produced an interesting model for FU Orionis type eruptive activity. He shows that it is possible for rapidly rotating low-mass T Tauri stars contracting along their Hayashi tracks to become unstable to barlike deformations. This would cause conversion of rotational energy to heating in the outer layers, causing matter ejection and loss of angular momentum to the star. During these phases, the star makes large excursions to higher luminosity and photospheric temperature on the H-R diagram. These excursions rapidly reach maximum luminosity, but decline over longer time scales. Herbig (1977) has argued from the number of FU Ori stars that the phenomenon is recurrent and must occur at least every 10^4 years. The fading time scale on Larson's models is uncertain, depending heavily on the model parameters, but in the case of V1057 Cyg could be estimated from observation to be $\sim$15 years, which implied a mass of 1.2 $M_\odot$. This time scale is interestingly close to the computed shock time scales in HH 47 and HH 43, and strengthens our argument that HH 46 contains within it a T Tauri star in a postoutburst phase.

There remain some problems with the shock models. Although the observational discrepancy between Hα/Hβ ratios has at last been resolved, there remains some uncertainty on the theoretical excitation rates for hydrogen. A full close-coupling treatment with interstate interaction is needed.

From the point of view of understanding the HH objects, a more fundamental problem is the observation of relatively strong high excitation UV resonance lines in HH 1 and 2 (Ortolani and D'Odorico 1980; Böhm, Böhm-Vitense, and Brugel 1981). According to these authors it is not possible to explain the UV and optical emission line intensities by a superposition of, say, a hot (UV emitting) shock and a cool (visibly radiating) shock. To explain the strength of the UV lines, the visible [O III] and [Ne III] intensities resulting would be much higher than observed. Böhm, Böhm-Vitense, and Brugel (1981) speculate that the higher excitation UV lines might arise in a hot, dense medium in which forbidden lines are quenched, while the optical lines arise in cooler, lower density regions. This would imply that the UV lines come from a much higher pressure region, but this leads to problems in the geometrical interpretation. In our models, the UV lines are predicted to be weak in high-excitation HH objects and negligible in the low-excitation ones. It would be useful to obtain UV observations of the latter type of objects to determine if they too exhibit enhanced UV emission lines and to confirm the predicted strong $2q$ continuum.

One of us (R. D. S.) acknowledges support of a University of Missouri Weldon Spring research award and also a Visiting Fellowship from Mount Stromlo and Siding Spring Observatories. Publication of this work was made possible by NSF grant AST 80-02407.

REFERENCES

Barral, J. F., and Cantó, J. 1981, *Rev. Mexicana Astr. Ap.*, **5**, 101.
Benvenuti, P., Dennefeld, M., D'Odorico, S., Dopita, M. A., and Greve, A. 1980, *Astr. Ap.*, **92**, 22.
Böhm, K. H., Böhm-Vitense, E., and Brugel, E. W. 1981, *Ap. J. (Letters)*, **245**, L113.
Böhm, K. H., Brugel, E. W., and Mannery, E. 1980, *Ap. J. (Letters)*, **235**, L137.
Böhm, K. H., Schwartz, R. D., and Siegmund, W. A. 1974, *Ap. J.*, **193**, 353.
Boksenburg, A. 1972, *Proc. ESO/CERN Conf. on Auxiliary Instrumentation for Large Telescopes*, Geneva, May 2–5, p. 295.
Brocklehurst, M. 1971, *M.N.R.A.S.*, **153**, 471.
Brown, R. L., and Mathews, W. G. 1970, *Ap. J.*, **160**, 939.
Brugel, E. W., Böhm, K. H., and Mannery, E. 1981*a*, *Ap. J.*, **243**, 874.
———. 1981*b*, *Ap. J. Suppl.*, **47**, 117.
Burke, P. G., Ormonde, S., and Whitaker, W. 1967, *Proc. Phys. Soc.*, **92**, 319.
Cantó, J. 1980, *Astr. Ap.*, **86**, 327.
Cantó, J., and Rodriguez, L. F. 1980, *Ap. J.*, **239**, 982.
Cantó, J., Rodriguez, L. F., Barral, J. F., and Carrol, P. 1981, *Ap. J.*, **244**, 102.
Capriotti, E. R. 1965, *Ap. J.*, **142**, 1101.

Cohen, M., and Kuhi, L. V. 1979, *Ap. J. Suppl.*, **41**, 743.
Dopita, M. A. 1978, *Ap. J. Suppl.*, **37**, 117.
———. 1981, in *Exploring the Universe: Papers in Honor of Z. Kopal* (Dordrecht: Reidel).
Herbig, G. H. 1977, *Ap. J.*, **217**, 693.
Herbig, G. H., and Jones, B. F. 1981, *A.J.*, **86**, 1232.
Imhoff, C. L., and Mendoza, E. E. 1974, *Rev. Mexicana Astr. Ap.*, **1**, 25.
Johnson, L. C. 1972, *Ap. J.*, **174**, 227.
Joy, A. H. 1945, *Ap. J.*, **102**, 168.
Kleinpoppen, H., and Kraiss, E. 1967, *Phys. Rev. Letters*, **20**, 361.
Larson, R. D. 1980, *M.N.R.A.S.*, **190**, 321.
Miller, J. S. 1968, *Ap. J.* (*Letters*), **154**, L57.
Moore, C. E. 1945, *A Multiplet Table of Astrophysical Interest* (Princeton Univ. Contrib. No. 20).
Oke, J. B. 1974, *Ap. J. Suppl.*, **27**, 21.
Ortolani, S., and D'Odorico, S. 1980, *Astr. Ap.*, **83**, L8.
Osterbrock, D. E. 1974, *Astrophysics of Gaseous Nebulae* (San Francisco: Freeman).
Pengelly, R. M., and Seaton, M. J. 1964, *M.N.R.A.S.*, **127**, 165.
Pradhan, A. K. 1976, *M.N.R.A.S.*, **177**, 31.
Pravdo, S. H., and Marshall, F. E. 1981, *Ap. J.*, **248**, 591.
Raymond, J. C. 1979, *Ap. J. Suppl.*, **39**, 1.
Schmidt, G., and Miller, J. S. 1979, *Ap. J.* (*Letters*), **234**, L191.
Schwartz, R. D. 1975, *Ap. J.*, **195**, 631.
———. 1976, *Pub. A.S.P.*, **88**, 159.
———. 1977, *Ap. J.* (*Letters*), **212**, L25.
Schwartz, R. D., and Dopita, M. A. 1980, *Ap. J.*, **236**, 543.
Shull, M., and McKee, C. F. 1979, *Ap. J.*, **227**, 131.
Strom, K. M., Strom, S. E., and Kinman, T. D. 1974, *Ap. J.* (*Letters*), **191**, L93.

L. BINETTE and M. A. DOPITA: Mount Stromlo and Siding Spring Observatories, Private Bag, Woden P.O., A.C.T. 2606, Australia

RICHARD SCHWARTZ: Department of Physics, College of Arts and Sciences, University of Missouri—St. Louis, 8001 Natural Bridge Road, St. Louis, MO 63121